A MODEL-BASED WIND ESTIMATION METHOD FOR AN UNMANNED HELICOPTER

Sergey Nazarov, Technion - Israel Institute of Technology, Haifa, Israel
Per-Olof Gutman, Technion - Israel Institute of Technology, Haifa, Israel

Abstract

Atmospheric wind and turbulence significantly affect flight efficiency, control performance, and safety. This paper describes a new original in-flight algorithm for wind/turbulence field estimation using a standard unmanned rotorcraft sensor kit and control signals produced by the flight control system. A linear identified model is proposed as a basic model of helicopter dynamics. This model is modified into a quasi-nonlinear model by adding trim data and nonlinear kinematic equations. A nonlinear Unscented Kalman Filter is designed using the quasi-nonlinear model and the scaled unscented transformation to estimate wind components in the North-East-Down frame. The resulting estimate is split using moving averaging into the steady horizontal wind and atmospheric turbulence. This algorithm has been tested on a continuous model-stitched simulation in which the wind and atmospheric turbulence simulated by the Dryden model have been added. The result was also validated by an actual Steadicopter Black Eagle (BE-50) unmanned helicopter flight test.

1. NOTATION

Symbols:

A,B,G	Linear system, control and gust matrices
a_x,a_y,a_z	Accelrometer components, m/s^2
C_x	Cholesky factor
$\boldsymbol{F}$	Continuous nonlinear process function
$\boldsymbol{F}_g$,$\boldsymbol{F}_a$	Total gravity and aerodynamic forces, N
$\bar{\boldsymbol{F}}_g$,$\bar{\boldsymbol{F}}_a$	Specific gravity and aerodynamic forces, m/s^2
$\boldsymbol{F}_I$	Total external force, N
g	Acceleration of gravity, m/s^2
$\boldsymbol{H}$	Nonlinear observation function
$\boldsymbol{H}$	Angular momentum, N·m·s
$\boldsymbol{I}$	Inertia tensor, kg·m^2
$\boldsymbol{K}$	Kalman gain
L	Turbulence length scale, m
L,M,N	External moments about CG, N·m
$L_{(\cdot)}$,$M_{(\cdot)}$,$N_{(\cdot)}$	Roll, pitch and yaw derivatives, 1/(m·s), 1/s, 1/s^2
$L_{\beta_{1s}}$,$N_{\beta_{1c}}$	Rotor flap-stiffness constants, 1/s^2
$\boldsymbol{M}_a$	Total aerodynamic moment, N·m
m,m_c	Helicopter base and current mass, kg
$P_{(\cdot)}$	Covariance matrix
P,Q,R	Total rates (roll, pitch, yaw), rad/s
p,q,r	Rate perturbations, rad/s
$\boldsymbol{Q}$	Process noise covariance
$\boldsymbol{R}$	Measurement noise covariance
R	Rotor radius, m
$\boldsymbol{r}$	Aircraft position radius vector, m
r	Rotor disk radial coordinate, m
S	Autospectral density function
$\boldsymbol{S}_I^B$	Inertial to body DCM matrix
t,t_s	Time and sampling interval, s
U,V,W	Body velocity components, m/s
$\boldsymbol{U}_d$	Delayed control vector
U_w,V_w,W_w	Wind in the body frame, m/s
u,v,w	Body velocity perturbations, m/s
$\boldsymbol{V}_B$	Velocity referred to the body axis, m/s
$\boldsymbol{V}_I$	Total inertial velocity, m/s
V_i,$\boldsymbol{V}_a$	Indicated and true airspeed, m/s
V_N,V_E,V_D	Velocity in the NED frame, m/s
$\boldsymbol{V}_{wind}$	Wind referred to the body axis, m/s

$\boldsymbol{v}$	Measurement noise vector
$\boldsymbol{v}_d$	Measurement noise in discrete time
$\boldsymbol{W}$	Navigational wind vector, m/s
$\boldsymbol{W}_{\text{meteo}}$	Meteorological wind vector, kt
W_N,W_E,W_D	Wind in the NED frame, m/s
$\boldsymbol{w}$	Process noise vector
$\boldsymbol{w}_d$	Process noise in discrete time
w_x,w_y,w_z	Turbulence components in the wind-related coordinate system, m/s
$\boldsymbol{X}$,$\boldsymbol{U}$	Total state and control vectors
$\boldsymbol{X}_0$,$\boldsymbol{U}_0$	Trim state and control vectors
$X_{(\cdot)}$,$Y_{(\cdot)}$,$Z_{(\cdot)}$	Forces derivatives, 1/s, m/s, m/s^2
$X_{\beta_{1c}}$,$Y_{\beta_{1s}}$	Force flap stiffness, m/s^2
$\boldsymbol{x}$,$\boldsymbol{u}$	Perturbed state and control vectors
x,y,z	Aircraft position, m
x_a,y_a,z_a	IMU position offset, m
$\boldsymbol{Z}$	Measurement vector
β	Flap angle, rad
β_0,β_{1c},β_{1s}	Flap angles for coning, longitudinal and lateral tip path plane, rad
γ	Lock number
δ_{col},δ_{ped}	Collective and pedals controls, rad
δ_{lat},δ_{lon}	Cyclic controls, rad
κ	Tuning factor
λ	Rotor inflow ratio
λ_w	Nondimentional vertical turbulence
μ	Advanced ratio
ν_β	Natural flapping frequency in term of the rotational speed, nondimentional
$\sigma_{\tilde{W}}$,$\sigma_{\tilde{\Psi}_W}$	Standard deviation of wind and its direction estimation error, kt, deg
$\sigma_{\tilde{W}_N}$,$\sigma_{\tilde{W}_E}$ $\sigma_{\tilde{W}_N}$	Wind components estimation error standard deviation, m/s
σ_{w_x},σ_{w_y}, σ_{w_z}	Standard deviation of turbulence components, m/s
$\boldsymbol{\tau}$	Equivalent delay vector, s
τ_f,τ_s	Rotor flap and flybar time constants, s
$\boldsymbol{\Phi}$	Discrete nonlinear process function
Φ,Θ,Ψ	Absolute attitudes (roll, pitch, yaw), rad
ϕ,θ,ψ	Attitude perturbations, rad
Ψ	Azimuth angle of blade, rad
Ω	Rotor rotation speed, rad/s
Ω	Spatial frequency, rad/m
$\boldsymbol{\omega}$	Angular velocity vector, rad/s

Acronyms:

AGL	(Height) Above Ground Level
AMSL	(Height) Above Mean Sea Level
CG	Center of Gravity
DCM	Direction Cosine Matrix
IAS	Indicated Airspeed
ICAO	International Civil Organisation
IMU	Inertial Measurement Unit
INS	Inertial Navigation System
EKF	Extended Kalman Filter
ENU	East-North-Up
GPS	Global Positioning System
GS	Ground Speed
MA	Moving Average
MMSE	Minimum Mean Square Error
NED	North-East-Down
TAS	True Airspeed
UA	Unmanned Aircraft
UAS	Unmanned Aircraft System
UKF	Unscented Kalman Filter
UT	Unscented Transformation

2. INTRODUCTION

The rapid development of Unmanned Aircraft Systems (UASs) in the past three decades makes it possible to use them in various human activity fields. The growing demands on applications stimulate the further development of UAS technologies, especially regarding civil tasks for which flight safety is the main objective. The wind and the atmospheric turbulence impose restrictions on unmanned rotorcraft operations. The magnitude, frequency content, and dimensions of atmospheric flow are expected to affect the rotary Unmanned Aircraft (UA) dynamics, control performances, and flight safety. The autopilot control laws may change significantly to achieve good performances in a turbulent atmosphere (Ref. 1). The wind nonlinearly affects the guidance algorithm and strongly affects the spatial orientation and rates of the small UA. The guidance laws should be modified to consider wind influence when flying in strong winds (Ref. 2). Since the pilot is not on board the UA, estimating turbulence level and wind and informing the ground control station should occur automatically. Moreover, this estimate is also directly required for civilian UASs by Circular 328 of ICAO (see Ref. 3). Therefore, methods that reasonably determine wind conditions are of unquestioned interest. The rotary UA with sensors directly measuring wind/turbulence intensity can solve this problem. Nevertheless, the main rotor downwash can produce substantial distortions in the measurement. Moreover, not all unmanned rotorcraft can be equipped with such sensors because of payload limitations and their high cost.

The classic method for the fixed wing consists of using the wind triangle. The wind can be estimated if the true airspeed (TAS) is known from the air data system and the ground speed (GS) vector is known from the navigation system. For instance, circular flight patterns are used in Reference 4, and the speed and direction of the wind are estimated by minimization of error variance. In other studies (Ref. 5 and Ref. 6), the Extended Kalman filter (EKF) is used. However, all these methods assume TAS is known, while most small UAs are not equipped with angle-of-attack and side-slip sensors. In Reference 7, this problem is solved by estimating the correction factor, a function of the angle of attack and slip. However, it is also assumed that these angles are small. This assumption may be proper for fixed-wing aircraft, but it is unacceptable for a rotorcraft that can fly with high slip angles.

In the rotorcraft world, multi-copters stand out because the measurement of wind speed and direction is based on the aircraft tilts in the presence of wind. The identification is produced by the known kinematic model, the trust, and measured multi-copter angles (see Ref. 8). The wind effect on multi-copter is identified by direct force measurement in the lab (Ref. 9) or flight testing when the wind is known (Ref. 10). Most works consider only steady-state modes (hover or steady flight). A rare example of wind estimation for a single-rotor helicopter is Reference 11, using a complex nonlinear helicopter model. Particle Swarm Optimization is used to optimize 37 parameters of this model for hover conditions. This optimization is based on the measurement of translational and rotational acceleration. Subsequently, the model extracted wind parameters through anomalies in the helicopter dynamics estimates. However, it seems as if this method cannot be widely used in practice: In rotorcraft applications, first principles dynamics modeling includes several hard-to-determine analytically uncertain parameters (see Ref. 12).

Typically, turbulence estimation is considered separately from wind estimation in scientific studies. In the fixed-wing approach considering atmospheric turbulence for flight dynamics problems, several simplifying assumptions (see Ref. 13) are made, and vertical acceleration is used to reconstruct turbulence intensity (Ref. 14). However, the standard turbulence models are not always applicable to rotary-wing aircraft due to different flight regimes and aerodynamic conditions (low airspeed, rotating airfoil, see Ref. 15). For example, rotational velocity effects can be dominant for conventional helicopters ($\mu < 0.4$, see Ref. 16). For rotorcraft, because of the blades flapping, a significant fraction of the turbulence energy is damped, and the load factor at the center of gravity is lower than that of a fixed-wing airplane (Ref. 17). However, loads on the hub increase significantly. Vertical wind gusts can cause sharp changes in helicopter altitude, leading to a 5% change in the rotor speed (Ref. 18). These challenges make a turbulence reconstruction from the helicopter response non-trivial. Literature is sparse on this subject for rotorcraft. In Reference 19, a Kalman filter approach for gust identification by a small-scale helicopter is proposed. This work continues a series of studies of the equivalent airwake disturbances method at Penn State University. A 28-state linear model of open-loop helicopter dynamics was extracted from GenHel© for a trim condition (see Ref. 20). The model was simplified to a 9-states rigid body dynamics model to analyze equivalent disturbance. The wind gust disturbances are added to the helicopter model by a gust matrix G. The resulting terms in the G matrix differ substantially from the equivalent terms in the A matrix. However, finding the matrix G can be tricky. Significant modifications were made to the GenHel© model to get a linear G matrix. The gust identification algorithm uses only inertial IMU and pilot input measurements. This algorithm showed positive results in the primary flow axis, but the gust detection error was significant in the off-axis flow direction.

This research proposes a new in-flight algorithm using a standard UA sensor kit and control signals produced by the flight control system as the primary data for wind field reconstruction. This approach does not assume steady flight, like other existing methods. However, it remains to investigate the characteristics of flight and wind patterns for which the sought disturbance vector is observable. As a basic model of helicopter dynamics, a linear identified model is proposed, which is used for the flight control design and is available for all UAS projects. The BE-50 of Steadicopter Ltd, Israel, was chosen as the helicopter flight test platform. Linear models were identified and verified for several anchor points within the flight envelope. These discrete-point linear models and trim data were combined into a full flight-envelope simulation based on a comprehensive model stitching architecture. One linear forward-flight helicopter model is selected and modified into a quasi-nonlinear model by adding trim data and nonlinear kinematic equations. For the first time ever (as far as the authors could ascertain), a nonlinear Unscented Kalman filter is designed using the quasi-nonlinear helicopter model, and the scaled unscented transformation (UT) to estimate wind components in the North-East-Down (NED) frame. The resulting estimate is split using moving averaging into the steady horizontal wind and atmospheric turbulence.

This algorithm was tested on the continuous model-stitched simulation in which the wind and atmospheric turbulence simulated by the Dryden model were added. The components of the atmospheric fluctuation in the simulation were successfully estimated. The result was also validated by an actual BE-50 helicopter flight test.

The paper is organized as follows. First, the main idea is discussed, the helicopter model is described, and the atmospheric disturbances - helicopter dynamics interface is introduced. Next, it details the new method for wind/turbulence estimation. Finally, the simulation and flight test results are presented.

3. METHODOLOGY

3.1. Description of the Helicopter

The rotary UA used for research is the BE-50 of Steadicopter Ltd, Israel. All supported operations, like flight testing, implementation of suggested control actions, or path patterns, are provided by Steadicopter's engineers and pilots. The BE-50 uses a two-bladed teetering main rotor with a Bell-Hiller stabilizer bar (see Figure 1). The main characteristics of the helicopter are given in Table 1.

Figure 1: BE-50 helicopter

Table 1: BE-50 Main Characteristics

Parameter	Value
Maximum takeoff weight	50 kg
Maximum payload weight	15 kg
Engine type	Electric
Main rotor diameter	2.80 m
Total length	3.10 m
Max air speed	77 kt (39.61 m/s)
Cruising speed	45 kt (23.15 m/s)
Wind (takeoff and landing)	25 kt (12.86 m/s)
Service ceiling	18000 ft (5486 m)

3.2. Wind and Aviation Turbulence

In the broad sense, the wind is any air motion relative to the earth's surface. This motion has a turbulent nature. However, specific components of this motion are characterized by such large scales that they can be considered a motion with constant velocity from the flight dynamics point of view. The turbulent motion in the atmosphere includes a large spectrum of eddy sizes. Larger eddies cause only slow variations in the flight path, while the effect of tiny eddies is integrated over the aerodynamic surfaces. A subset within a limited range of the turbulence spectrum which affects an aerodyne in flight is called *aviation turbulence* (see Ref. 21). Therefore, the aircraft's reaction determines the spectrum of atmospheric fluctuations of interest.

Let us denote $\boldsymbol{r}(x, y, z, t)$ as the radius vector defining the position of the rotorcraft relative to the earth (the curvature of the earth is neglected). In this case, the wind affecting the rotorcraft flight dynamics can be written as

$$\boldsymbol{W}(\boldsymbol{r}, t) = \boldsymbol{W}_0(\boldsymbol{r}, t) + \boldsymbol{\delta W}(\boldsymbol{r}, t) \tag{1}$$

where $\boldsymbol{W}_0(\boldsymbol{r}, t)$ characterizes a very slowly varying component, which can be viewed as constant in a particular spatial region and over a specific time and called *steady wind*, and $\boldsymbol{\delta W}(\boldsymbol{r}, t)$ is a random component with constant statistical characteristics. In this work, we use the navigational wind vector in the NED frame

$$\boldsymbol{W} = \begin{bmatrix} W_N & W_E & W_D \end{bmatrix}^T \tag{2}$$

which can be converted into a meteorological wind vector $\boldsymbol{W}_{\text{meteo}}$, or into body frame wind $\boldsymbol{V}_{\text{wind}}$ using a transformation matrix. In aviation, the steady wind is defined as the movement of air *parallel* to the earth's surface ($\boldsymbol{W}_0 = [W_{N_0}\ W_{E_0}\ 0]$, see Ref. 22).

3.3. The Main Idea of this Work

The rotorcraft's position relative to an inertial rectangular coordinate system is described by the differential equation

$$\frac{\mathrm{d}\boldsymbol{r}}{\mathrm{d}t} = \boldsymbol{V}_I = \boldsymbol{V}_a + \boldsymbol{W}(\boldsymbol{r}, t) \tag{3}$$

where $\boldsymbol{V}_I$ is an inertial velocity, $\boldsymbol{V}_a$ is a true airspeed and $\boldsymbol{W}$ is a wind vector. All velocities here are defined relative to the rotorcraft's center of gravity (CG). The challenge is to find the wind when the true airspeed is unknown. In equation (3) there are two unknowns, but on the other hand, the changes in inertial velocity $\boldsymbol{V}_I$ depend on changes in aerodynamic force, which is a function of the true airspeed $\boldsymbol{V}_a$. Newton's second law describes the rotorcraft's CG translational motion as

$$\frac{\mathrm{d}\left(m\boldsymbol{V}_I\right)}{\mathrm{d}t} = \boldsymbol{F}_I \tag{4}$$

where $\boldsymbol{F}_I$ is the total external force vector in the inertial frame. For a body-fixed coordinate system, this equation can be rewritten as

$$\frac{\partial \boldsymbol{V}_B}{\partial t} + \boldsymbol{\omega} \times \boldsymbol{V}_B = \bar{\boldsymbol{F}}_g + \bar{\boldsymbol{F}}_a\left(\boldsymbol{V}_a\right) \tag{5}$$

where $\boldsymbol{V}_B = U\boldsymbol{i} + V\boldsymbol{j} + W\boldsymbol{k}$ is velocity vector expressed in components in the body axis, $\boldsymbol{\omega} = P\boldsymbol{i} + Q\boldsymbol{j} + R\boldsymbol{k}$ is the angular velocity vector of the body-fixed axis system, $\bar{\boldsymbol{F}}_g$ and $\bar{\boldsymbol{F}}_a$ are specific gravity and aerodynamic forces in body frame. The velocity vector referred to the body frame is related to the inertial velocity vector through the direction cosine matrix (DCM).

$$\boldsymbol{V}_B = \boldsymbol{S}_I^B \boldsymbol{V}_I \tag{6}$$

The specific aerodynamic force $\bar{\boldsymbol{F}}_a\left(\boldsymbol{V}_a\right)$ is a function of the true airspeed due to basic aerodynamics, and the gravity force is a function of the angular orientation of the rotorcraft relative to the earth's surface. The moment equation expressed in a body-fixed frame is

$$\frac{\partial \boldsymbol{H}}{\partial t} + \left(\boldsymbol{\omega} \times \boldsymbol{H}\right) = \boldsymbol{M}_a\left(\boldsymbol{V}_a\right) \tag{7}$$

where $\boldsymbol{H} = \boldsymbol{I}\,\boldsymbol{\omega}$, is an angular momentum $\boldsymbol{I}$ is an inertia tensor and $\boldsymbol{M}_a\left(\boldsymbol{V}_a\right)$ is a vector of total aerodynamic moment which is also a function of true airspeed. If we can model aerodynamic forces and moments as a function of airspeed, we can use Equations (3) - (7) as a Kalman filter process model to estimate the wind $\boldsymbol{W}$. This model forms part of the helicopter flight dynamics model.

3.4. Unmanned Rotorcraft Dynamics Modeling

There are two approaches to modeling rotorcraft dynamics. The first modeling approach involves deriving the equations of motion from the fundamental laws of mechanics and aerodynamics. This approach requires a priori knowledge of all parameters that affect the rotorcraft dynamics. However, a compressed development schedule of UASs compared to manned flight vehicles (6-12 months rather than 5-10 years, see Ref. 23) often precludes the physics-based modeling approach. Furthermore, wind tunnel experiments are expensive and time-consuming, and the equipment for carrying out such experiments is usually unavailable for most ordinary UAS projects. Therefore, determining the unmanned rotorcraft model using system identification methods is more convenient and workable.

The main goals of unmanned helicopter dynamics modeling are flight control design and flying qualities studies. Using linear models is helpful since numerous analysis and design techniques are available for linear systems. Therefore, it is preferable to identify the already linearized helicopter model. However, to cover the entire flight envelope, multiple linear models and multiple controllers are necessary (Ref. 24). The equations of the rotorcraft motion cast in the state-space form are

$$\dot{\boldsymbol{x}} = \boldsymbol{A}\boldsymbol{x} + \boldsymbol{B}\boldsymbol{u}\left(t - \boldsymbol{\tau}\right) \tag{8}$$

where a time delay vector $\boldsymbol{\tau}$ expresses the unmodeled high-order dynamics and the equivalent delay in the mechanical and electrical parts of the control system. The size of the state vector depends on the dynamics of a specific helicopter and the particular task. Typically, small-scale helicopters have low damping coupled fuselage-rotor flapping dynamics, and a coupled rotor-body model is required. The state and control vectors used in (8) are

$$\begin{aligned} \boldsymbol{x} &= \left[\begin{array}{ccccccccccc} u & v & w & p & q & r & \phi & \theta & \psi & \beta_{1c} & \beta_{1s} \end{array} \right]^T, \\ \boldsymbol{u} &= \left[\begin{array}{cccc} \Delta\theta_{ped} & \Delta\theta_{lat} & \Delta\theta_{lon} & \Delta\theta_{col} \end{array} \right]^T \end{aligned} \tag{9}$$

where β_{1c} and β_{1s} are the rotor flap angles for longitudinal and lateral tip path plane coordinates. In this project, following Reference 23, we use a hybrid formulation of coupled fuselage-rotor flapping dynamics when the time constant of blade flapping is replaced by the time constant of the flybar.

$$\begin{aligned} \tau_s\dot{\beta}_{1c} &= -\beta_{1c} + M_{f_{\beta_{1s}}}\beta_{1s} + \tau_s q + \\ &\quad + M_{f_{\delta_{lon}}}\Delta\delta_{lon} + M_{f\,\delta_{lat}}\Delta\delta_{lat} \\ \tau_s\dot{\beta}_{1s} &= -\beta_{1s} + L_{f_{\beta_{1c}}}\beta_{1c} + \tau_s p + \\ &\quad + L_{f_{\delta_{lon}}}\Delta\delta_{lon} + L_{f_{\delta_{lat}}}\Delta\delta_{lat} \end{aligned} \tag{10}$$

The flapping is coupled to fuselage dynamics as

$$\begin{aligned} \dot{u} &= X_u u + X_v v + ... + X_{\beta_{1c}}\beta_{1c} \\ \dot{v} &= Y_u u + Y_v v + ... + Y_{\beta_{1s}}\beta_{1s} \\ \dot{p} &= L'_u u + L'_v v + ... + L_{\beta_{1s}}\beta_{1s} \\ \dot{q} &= M_u u + M_v v + ... + M_{\beta_{1c}}\beta_{1c} \end{aligned} \tag{11}$$

3.5. Model Identification and Validation

The parametric model was identified using the frequency domain method detailed in Reference 23. This system identification uses the frequency-response method implemented in the CIFER© package. The overall concept is to extract a complete set of non-parametric input-to-output frequency responses that fully characterize the coupled behavior of the system without a priori assumptions and conduct a nonlinear search for a state-space model that matches the input/output frequency-response data set. The low-frequency speed derivatives are identified from static stability flight tests.

3.6. Total Aerodynamic Force and Moment Calculation from Linear Model

The procedure for calculating aerodynamic forces and moments from the identified linear model is similar to the algorithm used in the model stitching simulation (see Ref. 25). From the identified model, we use only stability and control derivatives associated with aerodynamic forces and moments to calculate linear and angular accelerations, which, when multiplied by the mass/inertia matrix, give perturbations of the aerodynamic forces and the total aerodynamic moments. To get the total aerodynamic force vector, we should add its trim value, which numerically equals the gravity force in trim flight. This procedure is detailed below in the Appendix. However, a critical remark should be made. The total aerodynamic forces and moments calculated from the linear model are valid for the altitude close to the altitude for which this model was identified. These aerodynamic forces and moments can be scaled by the air density ratio for a fixed-wing aircraft. Nevertheless, the derivatives do not scale linearly with air density for rotorcrafts (see Ref. 25). Suppose the flight altitude varies significantly from that for which the models were obtained. In that case, it is e.g. necessary to interpolate the stability and control derivatives and trim data for two models obtained at different heights.

3.7. Atmospheric Disturbances - Helicopter Interface

The total time derivative of the wind at the moving point with velocity $\boldsymbol{V}_I$ is

$$\frac{d\boldsymbol{W}}{dt} = \frac{\partial \boldsymbol{W}}{\partial t} + \boldsymbol{V}_I \frac{\partial \boldsymbol{W}}{\partial \boldsymbol{r}} \tag{12}$$

Thus, the dynamic response of aircraft to the wind depends on the vehicle's speed and may be complicated. This work assumes that the wind velocity is uniformly distributed over the rotor disk. This assumption is valid for the appropriate ratio of turbulence length scale L and rotor radius (Ref. 26). In section 3.2, we defined aviation turbulence as the aircraft reaction. This spectrum of atmospheric disturbances includes large eddies that affect slow flight path fluctuations and small eddies that cause high-frequency vibrations. From a practical point of view, the most significant interest is caused by low and middle frequencies of atmospheric fluctuations that affect navigation, guidance, and control performance. Thus, in this work, we intend to estimate the wind (huge eddies) and medium-sized eddies affecting the control system. In this case, we can define the turbulence input in (8) as it is used in fixed-wing problems. Perturbations of aerodynamic forces and moments are calculated using the relative state vector.

$$[U\ V\ W]^T_{rel} = \boldsymbol{V}_B - \boldsymbol{V}_{\text{wind}} \tag{13}$$

where $\boldsymbol{V}_{\text{wind}} = [\ U_w \quad V_w \quad W_w\ ]^T$ is the wind referred to the body frame. To consider the effect of turbulence on high-order dynamics, we use the known flapping equation from Reference 15.

$$\begin{aligned} &\overset{**}{\beta} + \frac{\gamma}{2}\left(\frac{1}{4} + \frac{\mu}{3}\sin\Psi\right)\overset{*}{\beta} + \\ &+ \left[\nu_\beta^2 + \frac{\gamma}{2}\left(\frac{\mu}{3}\cos\Psi + \frac{\mu^2}{4}\sin 2\Psi\right)\right]\beta = F(t) \end{aligned} \tag{14}$$

where β is a flap angle and $\overset{*}{\beta} = \partial\beta/\partial\Psi$. The forcing function, under our basic assumption (W_w is not a function of r), takes the form

$$\begin{aligned} &F(t) = \frac{-\gamma}{2\Omega R^4}\int_0^R \left(r^2 + \mu R r\sin\Psi\right) W_w(t)dr = \\ &= -\frac{\gamma}{2}\left(\frac{1}{3} + \frac{\mu}{2}\sin\Psi\right)\lambda_w \end{aligned} \tag{15}$$

where λ_w is a non-dimensional vertical turbulence velocity. In (10), we use the linear helicopter model's hybrid formulation of coupled fuselage-rotor flapping dynamics. This model describes the flap angle dynamics from control input with the flay-bar time constant $\tau_s = 0.177$ sec. The dynamics of flapping from the wind disturbances are much faster and determined by the time constant of the rotor $\tau_f = 0.024$ sec. Therefore, for our task, instead of Equation (14), we use its steady-state periodic solution (with assumption $\nu_\beta^2 = 1$, see Ref. 27).

$$\begin{aligned} \Delta\beta_0 &= -\frac{\gamma}{6}\lambda_w \\ \Delta\beta_{1s} &= -\left(\frac{8}{3}\right)\frac{\mu\Delta\beta_0}{2+\mu^2} \\ \Delta\beta_{1c} &= -\frac{4\mu}{\mu^2-2}\lambda_w(t) \end{aligned} \tag{16}$$

where $\Delta\beta_0$, $\Delta\beta_{1s}$ and $\Delta\beta_{1c}$ deviation coning and flapping angles from trim values due to turbulence. Combining the first two equations, we get

$$\begin{bmatrix}\Delta\beta_{1c} \\ \Delta\beta_{1s}\end{bmatrix} = \begin{bmatrix} -\dfrac{4\mu}{\mu^2-2} \\ \left(\dfrac{4}{9}\right)\dfrac{\mu\gamma}{2+\mu^2}\end{bmatrix}\lambda_w \tag{17}$$

Finally, to calculate the total aerodynamic forces and moments, we use the sum of flap angles perturbation from control (10) and disturbance (17).

$$\begin{bmatrix}\beta_{1s} \\ \beta_{1s}\end{bmatrix}_{total} = \begin{bmatrix}\Delta\beta_{1s} \\ \Delta\beta_{1s}\end{bmatrix}_{wind} + \begin{bmatrix}\beta_{1s} \\ \beta_{1s}\end{bmatrix}_{control} \tag{18}$$

3.8. The Scaled Unscented Transformation

Let $\boldsymbol{x}$ be a n-dimensional random variable with the mean $\bar{\boldsymbol{x}}$ and covariance $\boldsymbol{P_x}$. Let also $\boldsymbol{y}$ be a random variable related to $\boldsymbol{x}$ through the nonlinear transformation

$$\boldsymbol{y} = \boldsymbol{\Phi}(\boldsymbol{x}) \tag{19}$$

The objective is to calculate the mean $\bar{\boldsymbol{y}}$ and covariance $\boldsymbol{P}_y$. We assume Gaussian distribution and generate a set of $\mathcal{O}(n)$ points having the same covariance from the columns of the matrix $\boldsymbol{P}_x$. The points should be positive and negative roots. This set of points is zero-mean, but by adding $\bar{\boldsymbol{x}}$ to each point we get a symmetric set of $2n$ points having desired mean and covariance. These points can be weighted by $\mathcal{W}$, such that $\sum_0^p W_i = 1$, where p is the total number of points.

We can use the Cholesky, or any other stable decomposition of the covariance matrix.

$$\boldsymbol{P}_x = \boldsymbol{C}_x\boldsymbol{C}_x^T \tag{20}$$

The basic symmetric sampling method consists of choosing $2n$ points in the addition of one point equalling the mean in the following way (it is also called *General unscented transformation*, Ref. 28)

$$\begin{aligned} \mathcal{X}_0 &= \bar{\boldsymbol{x}} \\ \mathcal{X}_i &= \bar{\boldsymbol{x}} + \sqrt{n+\kappa}\,\boldsymbol{C_x}(i) \quad 1 \le i \le n \\ \mathcal{X}_i &= \bar{\boldsymbol{x}} - \sqrt{n+\kappa}\,\boldsymbol{C_x}(i) \quad n+1 \le i \le 2n \end{aligned} \tag{21}$$

where the weights are $\mathcal{W}_0 = \kappa/(n+\kappa)$ and $\mathcal{W}_i = 1/2(n+\kappa)$, and κ is a tuning parameter. If the set of weighted sigma points $\mathcal{S} = (\mathcal{W}, \mathcal{X})$ has been derived, the prediction is straightforward (Ref. 29).

$$\mathcal{Y} = \boldsymbol{\Phi}\{\mathcal{X}\} \tag{22}$$

The mean is given by weighted average of the transformed points.

$$\bar{\boldsymbol{y}} = \sum_{i=0}^{p} W_i\mathcal{Y}_i \tag{23}$$

where $p = 2n + 1$ is a total number of points. The covariance is the weighted outer product of the transformed points.

(24) $$\boldsymbol{P}_y = \sum_{i=0}^{p} W_i \left(\mathcal{Y}_i - \bar{\boldsymbol{y}}\right)\left(\mathcal{Y}_i - \bar{\boldsymbol{y}}\right)^T$$

Because the set is symmetric its odd central moments are zero, so its first three moments are the same as the original. The UT can be directly extended to create the Unscented Kalman Filter (UKF) algorithm for the state estimation in nonlinear systems (see Ref. 30).

4. WIND ESTIMATION ALGORITHM

4.1. Nonlinear Process Model

We define the augmented state as

$$\boldsymbol{X^a} = \Big[U\ V\ W\ P\ Q\ R\ \Phi\ \Theta\ \Psi\ \beta_{1c}\ \beta_{1s}\ W_N\ W_E\ W_D\Big]^T$$

The nonlinear process function is

(25) $$\dot{\boldsymbol{X}}^{\boldsymbol{a}}(t) = \boldsymbol{F}\Big\{\boldsymbol{X^a}(t), \boldsymbol{U}(t-\boldsymbol{\tau})\Big\} + \boldsymbol{w}(t)$$

where $\boldsymbol{w}$ is an additive process noise, and $\dot{\boldsymbol{X}}^{\boldsymbol{a}}$ is assumed to have the following form

$$\dot{\boldsymbol{X}}^{\boldsymbol{a}} = \Big[\dot{U}\ \dot{V}\ \dot{W}\ \dot{P}\ \dot{Q}\ \dot{R}\ \dot{\Phi}\ \dot{\Theta}\ \dot{\Psi}\ \dot{\beta}_{1c}\ \dot{\beta}_{1s}\ 0\ 0\ 0\Big]^T$$

The nonlinear transformation $\boldsymbol{F}$ consists of calculating following equations

1. DCM $\boldsymbol{S}_I^B$ (52)
2. Wind in body frame $\boldsymbol{V}_{\text{wind}} = \boldsymbol{S}_I^B \boldsymbol{W}$
3. Relative velocity (13) and total flap angles (18)
4. Specific forces (36), (44) and total aerodynamic moment (49)
5. Nonlinear equations of motion (35), (47) and (50)
6. Linear equations of flapping (10)

4.2. Nonlinear Observation

The measurement vector consists of INS/GPS and Pitot data.

(26) $$\boldsymbol{Z} = \Big[P\ Q\ R\ a_x\ a_y\ a_z\ \Theta\ \Phi\ \Psi\ V_i\ V_N\ V_E\ V_D\Big]^T$$

where $[a_x\ \ a_y\ \ a_z]$ are the measured accelerations, V_i is an indicated airspeed and $\boldsymbol{V_I} = [V_N\ \ V_E\ \ V_D]^T$ is inertial velocity in the NED frame. The nonlinear observation function is

(27) $$\boldsymbol{Z}(t) = \boldsymbol{H}\Big\{\boldsymbol{X^a}(t), \boldsymbol{U}(t-\boldsymbol{\tau})\Big\} + \boldsymbol{v}(t)$$

where $\boldsymbol{v}$ is an additive measurement noise. Some components of the state vector are measured directly. The velocities in the body coordinate system are related to the inertial velocity in the NED frame through (6). The accelerometer measurements relative to the helicopter center of gravity are (Ref. 23)

(28) $$\begin{aligned} a_x &= \dot{U} + WQ - VR - \bar{X}_g + z_a\dot{Q} - y_a\dot{R} \\ a_y &= \dot{V} + UR - WP - \bar{Y}_g - z_a\dot{P} + x_a\dot{R} \\ a_z &= \dot{W} + VP - UQ - \bar{Z}_g + y_a\dot{P} - x_a\dot{Q} \end{aligned}$$

where x_a, y_a and z_a are the IMU location offsets relative to CG. The indicated speed corresponds to the relative velocity in the X_b direction.

(29) $$V_i = U - U_w$$

4.3. Estimation Problem Definition

First, let us discretize the process and the observation for a specific time step $\Delta t = t_s$. The filtering problem of interest is to find the MMSE linear estimate of the state vector $\boldsymbol{X^a}(k)$ of the system, which evolves according to the discrete-time nonlinear state transition equation.

(30) $$\begin{cases} \boldsymbol{X^a}(k{+}1) = \boldsymbol{\Phi}\Big\{\boldsymbol{X^a}(k), \boldsymbol{U}_d(k)\Big\} + \boldsymbol{w}_d(k) \\ \boldsymbol{Z}(k{+}1) = \boldsymbol{H}\Big\{\boldsymbol{X^a}(k{+}1), \boldsymbol{U}_d(k)\Big\} + \boldsymbol{v}_d(k{+}1) \end{cases}$$

We assume that $\boldsymbol{w}_d(k)$ and $\boldsymbol{v}_d(k)$ are Gaussian uncorrelated white sequences.

$$\mathbb{E}\left[\boldsymbol{w}_d(k)\right] = \boldsymbol{0}, \quad \mathbb{E}\left[\boldsymbol{v}_d(k)\right] = \boldsymbol{0}, \quad \mathbb{E}\left[\boldsymbol{w}_d(i)\boldsymbol{v}_d(j)^T\right] = \boldsymbol{0}$$

$$\mathbb{E}\left[\boldsymbol{w}_d(i)\boldsymbol{w}_d(j)^T\right] = \boldsymbol{Q}(i)\delta_{ij}$$

$$\mathbb{E}\left[\boldsymbol{v}_d(i)\boldsymbol{v}_d(j)^T\right] = \boldsymbol{R}(i)\delta_{ij}$$

4.4. Unscented Kalman Filter

We assume that the distribution of $\boldsymbol{X^a}(k)$ is Gaussian at any time k. The Kalman filter propagation of two moments of the distribution of $\boldsymbol{X^a}(k)$ incorporates linearly the measurements at the next time-step.

$$
(31)\quad \begin{cases} \hat{\boldsymbol{X}}^{\boldsymbol{a}}(k{+}1|k{+}1) = \hat{\boldsymbol{X}}^{\boldsymbol{a}}(k{+}1|k)\ + \\ \qquad\qquad + \boldsymbol{K}(k{+}1)\tilde{\boldsymbol{Z}}(k{+}1|k) \\ \boldsymbol{P}_x(k{+}1,k{+}1) = \boldsymbol{P}_x(k{+}1|k)\ - \\ \qquad\qquad -\boldsymbol{K}(k{+}1)\boldsymbol{P}_{\tilde{z}}(k{+}1|k)\boldsymbol{K}^T(k{+}1) \end{cases}
$$

where

$$
(32)\qquad \tilde{\boldsymbol{Z}}(k{+}1|k) = \boldsymbol{Z}(k{+}1) - \hat{\boldsymbol{Z}}(k{+}1|k)
$$

is the innovation with covariance $\boldsymbol{P}_{\tilde{z}}(k{+}1|k)$ and $\boldsymbol{K}$ is the Kalman gain

$$
(33)\qquad \boldsymbol{K}(k{+}1) = \boldsymbol{P}_{xz}(k{+}1|k)\boldsymbol{P}_{\tilde{z}}^{-1}(k{+}1|k)
$$

where $\boldsymbol{P}_{xz}$ is the predicted cross-correlation matrix between $\hat{\boldsymbol{X}}^{\boldsymbol{a}}(k{+}1|k)$ and $\hat{\boldsymbol{Z}}(k{+}1|k)$. We can calculate the predictions of state $\hat{\boldsymbol{X}}(k{+}1|k)$, measurement $\hat{\boldsymbol{Z}}(k{+}1|k)$ and covariance $\boldsymbol{P}_x(k{+}1|k)$, $\boldsymbol{P}_{\tilde{z}}(k{+}1|k)$, $\boldsymbol{P}_{xz}(k{+}1|k)$ using the UT (see Section 3.8). Since both transformations are nonlinear, using the UT allows us to avoid computing Jacobian and use the nonlinear model in its original form.

4.5. Summary of UKF algorithm

The implementation of the UKF for wind estimation consists of the following steps.

1. **Filter initialization**. We initialize with

$$
\boldsymbol{X}_0 = \begin{bmatrix} U_0 & 0 & W_0 & 0 & 0 & 0 & \Phi_0 & \Theta_0 & \Psi_0 & 0 & 0 \end{bmatrix}^T
$$

$$
\bar{\boldsymbol{X}}(0) = \mathbb{E}\left[\boldsymbol{X}_0\right]
$$

$$
\boldsymbol{P}_0 = \text{Cov}\left\{\boldsymbol{X}_0\right\}
$$

$$
\bar{\boldsymbol{X}}^{\boldsymbol{a}}(0) = \begin{bmatrix} \boldsymbol{X}_0^T & 0 & 0 & 0 \end{bmatrix}^T
$$

$$
\boldsymbol{P}_x(0) = \begin{bmatrix} \boldsymbol{P}_0 & 0 \\ 0 & \boldsymbol{P}_w(0) \end{bmatrix}
$$

   where $\boldsymbol{P}_w$ is a covariance of the wind components. During initialization, the control vector $\boldsymbol{U}_d(k)$ is delayed by the vector $\boldsymbol{\tau}$.

2. **Sigma point set calculation** $\mathcal{S} = (\mathcal{W}, \mathcal{X}^a(k|k))$.

3. **Prediction.** The stage of prediction consists of

   (a) Transformation each sigma point through the process

$$
\mathcal{X}_i^{\boldsymbol{a}}(k+1|k) = \boldsymbol{\Phi}\left\{\mathcal{X}_i^{\boldsymbol{a}}(k|k), \boldsymbol{U}_d(k)\right\}
$$

   (b) Prediction of the mean

$$
\hat{\boldsymbol{X}}^{\boldsymbol{a}}(k+1|k) = \sum_{i=0}^{2n^a} W_i \mathcal{X}_i^{\boldsymbol{a}}(k+1|k)
$$

   (c) Prediction of the covariance

$$
\boldsymbol{P}_x(k{+}1|k) = \sum_{i=0}^{2n^a} W_i \widetilde{\mathcal{X}}_i^{\boldsymbol{a}}(k{+}1|k)\left[\widetilde{\mathcal{X}}_i^{\boldsymbol{a}}(k{+}1|k)\right]^T + \boldsymbol{Q}(k)
$$

   where $\widetilde{\mathcal{X}}_i^{\boldsymbol{a}}(k{+}1|k) = \mathcal{X}_i^{\boldsymbol{a}}(k{+}1|k) - \hat{\boldsymbol{X}}^{\boldsymbol{a}}(k{+}1|k)$.

   (d) Transformation each sigma point through the observation model

$$
\mathcal{Z}_i(k+1|k) = \boldsymbol{H}\left\{\mathcal{X}_i^{\boldsymbol{a}}(k|k), \boldsymbol{U}_d(k)\right\}
$$

   (e) Computation the innovation covariance

$$
\boldsymbol{P}_z(k{+}1|k) = \sum_{i=0}^{2n^a} W_i \widetilde{\mathcal{Z}}_i(k{+}1|k)\left(\widetilde{\mathcal{Z}}_i(k+1|k)\right)^T
$$

   where $\widetilde{\mathcal{Z}}_i(k{+}1|k) = \mathcal{Z}_i(k{+}1|k) - \hat{\boldsymbol{Z}}(k{+}1|k)$.

$$
\boldsymbol{P}_{\tilde{z}}(k+1|k) = \boldsymbol{P}_z(k+1|k) + \boldsymbol{R}(k+1)
$$

   (f) Computation the cross correlation matrix

$$
\boldsymbol{P}_{xz}(k+1|k) = \sum_{i=0}^{2n^a} W_i \mathcal{X}_i^{\boldsymbol{a}}\left(\widetilde{\mathcal{Z}}_i(k+1|k)\right)^T
$$

4. **Filtering.** This stage is the regular one. We calculate the Kalman gain (33) and update the prediction (31). The prediction is updated for all components of the augmented state vector except for flap angles, for which only the prediction is used.

5. RESULTS AND DISCUSSION

5.1. Simulation

Performance of the UKF was tested by a BE-50 helicopter model-stitched simulation in the Matlab/Simulink environment©. The model-stitching architecture (Ref. 25) is similar to the nonlinear process model used in this work. However, the simulation consists of several linear models identified for different points inside a flight envelope. These models for discrete flight conditions were stitched with trim data to produce a continuous full flight envelope quasi-nonlinear simulation. Besides the helicopter dynamics model, the simulation includes models of navigation, guidance and flight control systems, actuator dynamics, and sensors. The atmospheric disturbances were modeled by Simulink blocks© of horizontal wind and the Dryden turbulence model. The simulation's interface between the wind and helicopter aerodynamics is the same as described in Section 3.7.

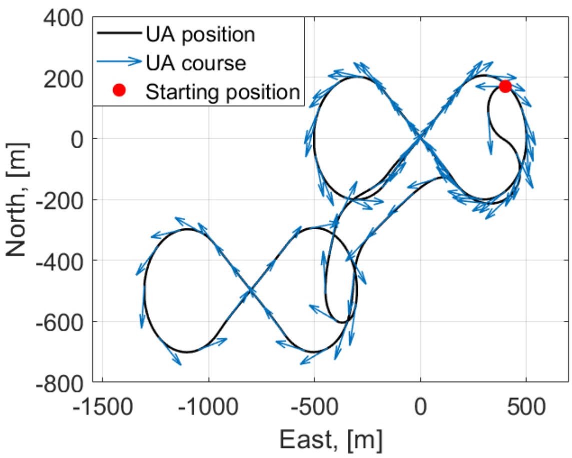

Figure 2: Flight pattern

The same conditions (altitude and airspeed) and helicopter configuration (mass) were chosen for the simulation as those for the nonlinear process model. The constant horizontal wind speed in the simulation was 10 knots (5.14 m/s) with a meteorological direction of 300 degrees. The helicopter flight was simulated with airspeed and altitude closed loops with commands of 30 knots (15.43 m/s) and 10 meters, respectively. The flight plan consists of two eight figures and transitions between them (see Figure 2). This flight plan includes straight flights, circles, and turns, suitable for testing the wind estimation algorithm. The simulation starts and ends at nearly the same point on the map and continues for 800 seconds with fixed-step integration $t_s = 0.001$ sec. The measurement noise covariance matrix $\boldsymbol{R}$ used in the UKF was known from the models of the sensors, and the process noise covariance was chosen as

$$\boldsymbol{Q} = \begin{bmatrix} 10^4 &&&&&&&&&&&&& \\ & 10^4 &&&&&&&&&&&& \\ && 10^4 &&&&&&&&&&& \\ &&& 10 &&&&&&&&&& \\ &&&& 10 &&&&&&&&& \\ &&&&& 10 &&&&&&&& \\ &&&&&& 10^{-5} &&&&&&& \\ &&&&&&& 10^{-5} &&&&&& \\ &&&&&&&& 10^{-5} &&&&& \\ &&&&&&&&& 10 &&&& \\ &&&&&&&&&& 10 &&& \\ &&&&&&&&&&& 10^{-7} && \\ &&&&&&&&&&&& 10^{-7} & \\ &&&&&&&&&&&&& 10^{-7} \end{bmatrix}$$

The filter was initialized with the first measurements received and the covariance was initialized as $\boldsymbol{P}_x(0) = \boldsymbol{Q}$.

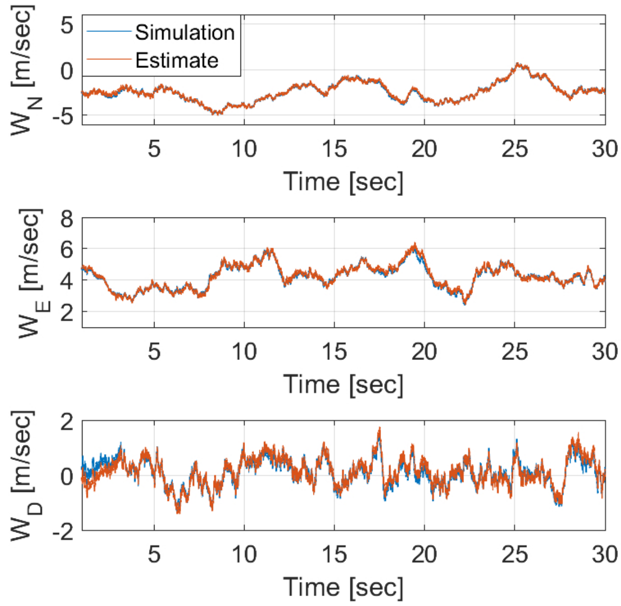

Figure 3: Simulation. Time domain: first 30 sec

A comparison of the simulated wind and its estimates is shown in Figure 3 and Figure 6. The estimate shows a high match with the simulation. However, we can observe an offset of 1.3 dB at low frequencies up to 1 rad/s for the vertical channel in the frequency domain (Figure 6c). However, the mean of the vertical wind estimation is close to zero.

$$\mathbb{E}[\hat{W}_D] = 0.01 \text{ m/s}$$

Since we used the same conditions in the simulation and the filter, such an offset is explained by the fact that the simulation's control and stability derivatives and trim values are looked up in tables. The simulation test for mass and height (air density) different from the values used in the filter leads to bias in the vertical estimate (nonzero mean). Fortunately, both parameters are always known for the present flight, and the issue is the change in derivatives and trim values with airspeed.

We used a moving average (MA) with a window of two minutes to estimate the constant wind component (see Figure 4 and Figure 5). The standard deviation of the error in estimating the meteorological wind direction using this MA is $\sigma_{\tilde{\Psi}_W} = 2.29$ degrees, and the

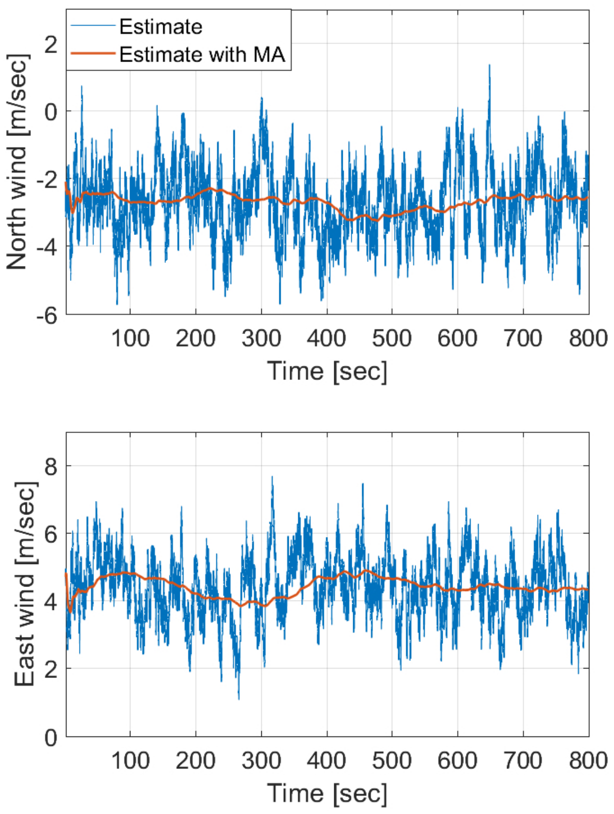

Figure 4: Simulation. Time domain with MA

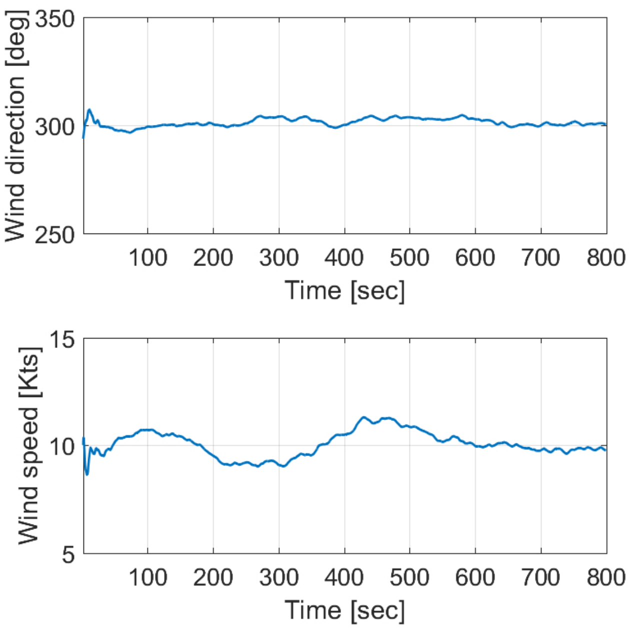

Figure 5: Simulation. Steady wind estimate

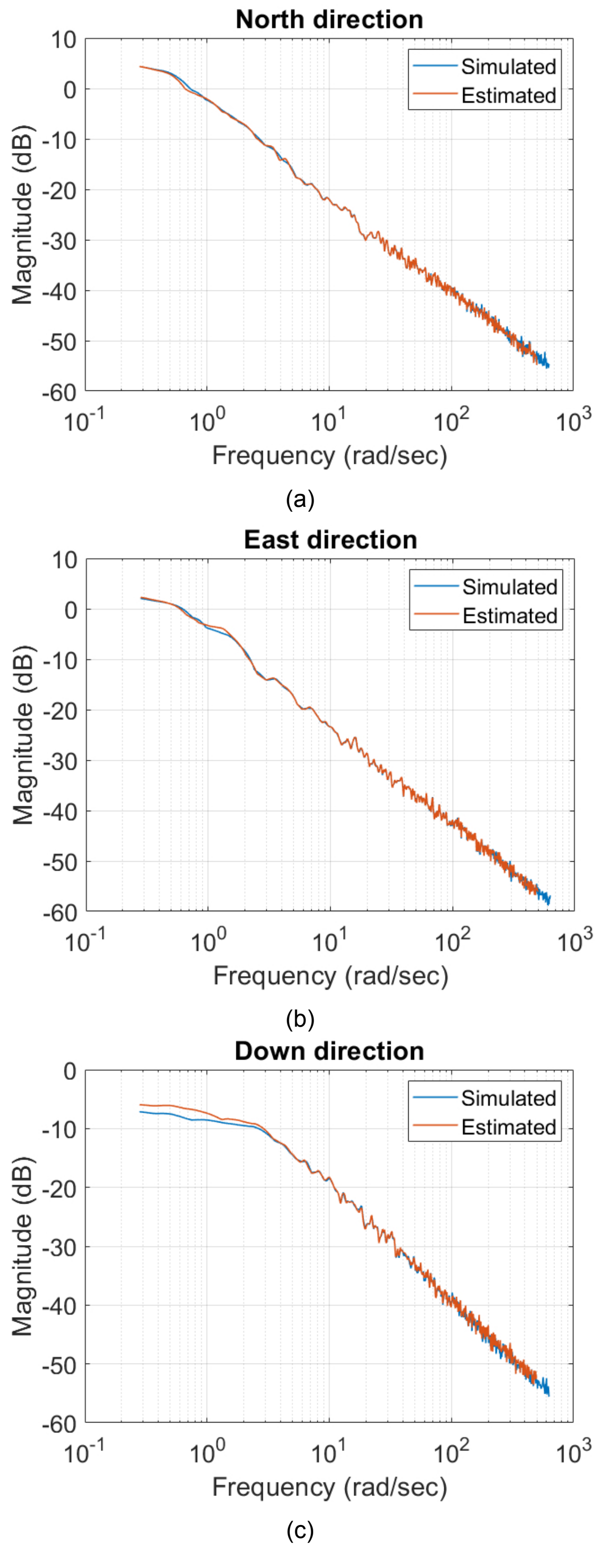

Figure 6: Simulation. Frequency domain

standard deviation of the wind velocity estimate error is $\sigma_{\tilde{W}} = 0.59$ Kts (0.3 m/s). Calculated standard deviations for the estimation error of the turbulence components are

$$\sigma_{\tilde{W}_N} = 0.10 \text{ [m/s]},\ \sigma_{\tilde{W}_E} = 0.09 \text{ [m/s]},\ \sigma_{\tilde{W}_D} = 0.11 \text{ [m/s]}$$

5.2. Flight test

The wind estimation algorithm was applied offline to the recorded flight test data. Only part of the flight at the airspeed of 30 knots was used. In this flight, the helicopter performed a helical figure with a radius of 150 meters and a change in altitude from 970 feet AMSL (230 feet AGL) to 1435 feet and back. The wind speed measured at the ground station is 9 knots, and its meteorological direction is West-Northwest. Since the sensor measurements are sent to the flight computer at a frequency of 100 Hertz, and the filter operates at 1000 Hertz, the algorithm has been slightly modified. Prediction continues to be calculated with the step $t_s = 0.001$, while the filtering calculates when the innovation comes. All other filter parameters remain the same as in the simulation.

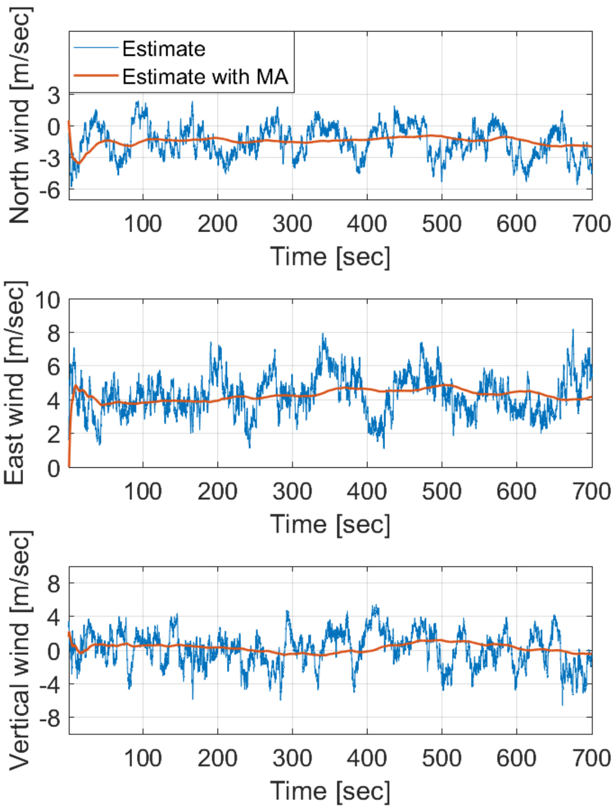

Figure 7: Flight test. Wind estimate

The estimation results are shown in Figure 7. We have used the MA with a three minutes window length. Figure 8 shows the calculated wind and direction from the averaged estimates. These two parameters are supposed to be downlinked to the ground station monitor. The values of the wind estimate and its meteorological direction are consistent with the measurements at the ground station.

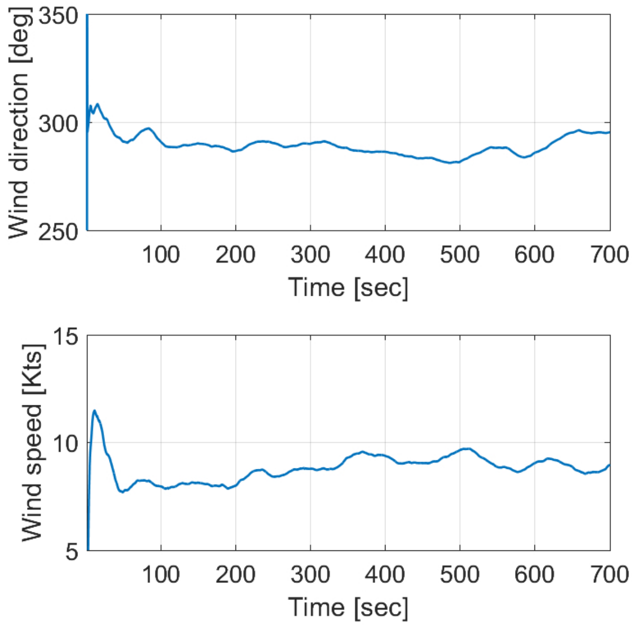

Figure 8: Flight test. Steady wind estimate

Figure 9 shows estimates of the turbulent component of the wind. It was obtained by subtracting the constant components from the wind estimate at a current moment. Then wind components were converted to local East-North-Up coordinates (ENU) and rotated by the wind angle so that the X-axis is directed along the navigational direction of the wind and Z-axis is pointing up.

We used the same moving time window of three minutes to compute the turbulence statistics. The estimated standard deviation of velocity in wind direction, the standard deviation of lateral velocity to the average wind direction, and the standard deviation of vertical wind component are shown in Figure 10. These values can also be transmitted to the ground station monitor to inform the operator of the existing turbulence. Alternatively, these estimates can be converted to standard turbulence levels; the current flight test estimates correspond to the ”Light” turbulence level (Ref. 21).

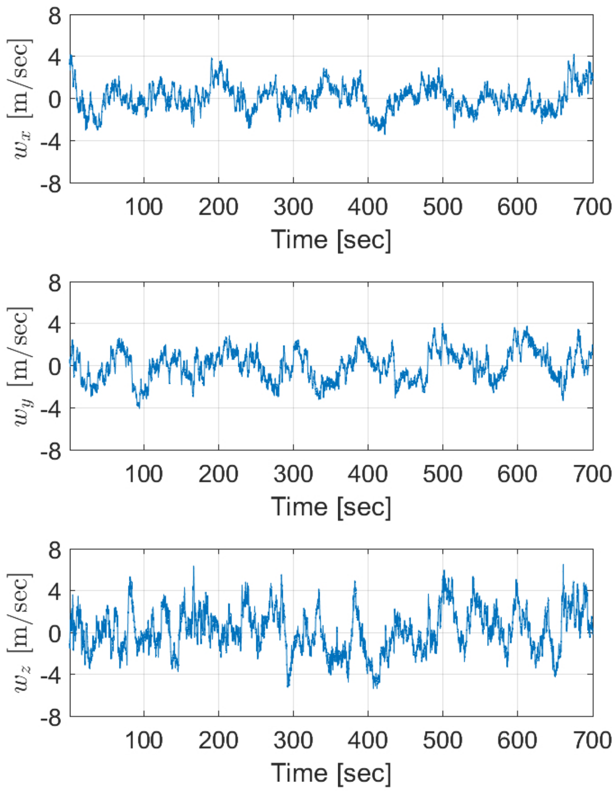

Figure 9: Flight test. Turbulence estimate

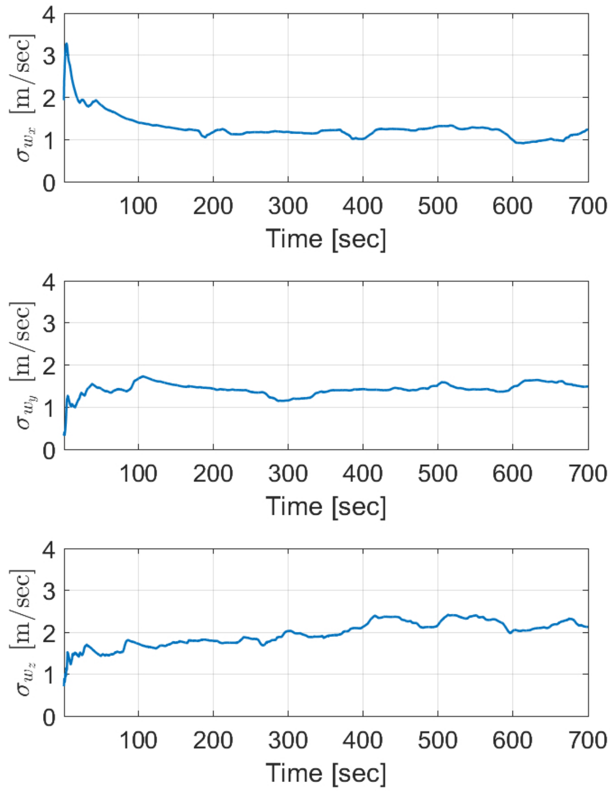

Figure 10: Flight test. Turbulence level estimate

The statistical characteristics of turbulence calculated for the all flight time are

$$\sigma_{w_x} = 1.24\,[\text{m/s}],\ \ \sigma_{w_y} = 1.46\,[\text{m/s}],\ \ \sigma_{w_z} = 2.07\,[\text{m/s}]$$

The energy spectrum of turbulence is shown in Figure 11. It can be concluded from the figure that the obtained turbulence characteristics correspond to the von Karman turbulence model up to 6.5 rad/s for the 30 knots flight speed. However, it should be remembered that the helicopter changed altitude. The turbulence characteristics can rapidly change with height near the ground.

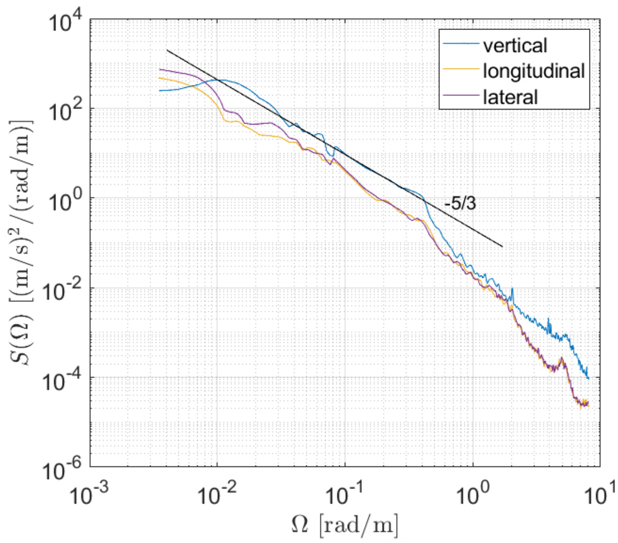

Figure 11: Flight test. Turbulence spectra estimate

6. CONCLUSIONS AND FUTURE WORKS

In this paper, a new practical method for wind estimating is proposed. The method is based on the identified helicopter linear model used for the flight control design and uses a standard UA sensor kit. Thus, the practical use of it is straightforward for any UAS project. The method allows UA to estimate wind speed and direction, as well as the level of turbulence. These data can be downlinked to the ground station monitor to inform the operator about critical wind characteristics at the current helicopter location. Using an Unscented Transform allows us to avoid computing Jacobian and use the nonlinear model in its original form. Since the total aerodynamic forces and moments are calculated inside the nonlinear process, this method is sensitive to the accuracy of mass, air density, and current airspeed parameters. Simulation and flight tests have shown that constant wind and its direction are estimated sufficiently, and the estimate's accuracy does not depend on the helicopter maneuver. However, offline calculations were used to validate the UKF in flight tests because it is still computationally expensive for the existing onboard computer and requires optimization. Counting the accuracy of the turbulent component estimate in flight tests is a practical challenge. However, the obtained flight test results can be approximated by the von Karman turbulence model up to 6.5 rad/s. In future work, the authors intend to find a technique to estimate the accuracy and compare the results with other turbulence models. The authors also intend to extend this method for low speeds and hover.

Author contact:

Sergey Nazarov sergey.n@campus.technion.ac.il

Per-Olof Gutman peo@technion.ac.il

7. APPENDIX

Force equations

The body-axis helicopter acceleration is given as

$$\frac{\partial \boldsymbol{V}_B}{\partial t} = -\left(\boldsymbol{\omega} \times \boldsymbol{V}_B\right) + \bar{\boldsymbol{F}}_g + \bar{\boldsymbol{F}}_a \tag{34}$$

The vector force equation can be rewritten in a scalar form and then it consists of the three force equations.

$$\begin{aligned} \dot{U} &= -QW + RV + \bar{X}_g + \bar{X}_a \\ \dot{V} &= -RU + PW + \bar{Y}_g + \bar{Y}_a \\ \dot{W} &= -PV + QU + \bar{Z}_g + \bar{Z}_a \end{aligned} \tag{35}$$

where specific gravity force vector is

$$\begin{bmatrix} \bar{X}_g \\ \bar{Y}_g \\ \bar{Z}_g \end{bmatrix} = \begin{bmatrix} -g \sin\Theta \\ g \sin\Phi\cos\Theta \\ g\cos\Phi\cos\Theta \end{bmatrix} \tag{36}$$

The specific aerodynamic force vector is calculated from the identified linear model of the helicopter. The linearized equations of helicopter motion are

$$\begin{aligned} \dot{u} &= -W_0 q + V_0 r - \left(g\cos\Theta_0\right)\theta + X_u u + \\ &\quad + X_v v + ... + X_{\delta_{ped}}\Delta\delta_{ped} + X_{\delta_{col}}\Delta\delta_{col} \\ \dot{v} &= -U_0 r + W_0 p + \left(g\cos\Theta_0\right)\phi + Y_u u + \\ &\quad + Y_v v + ... + Y_{\delta_{ped}}\Delta\delta_{ped} + Y_{\delta_{col}}\Delta\delta_{col} \\ \dot{w} &= -V_0 p + U_0 q - \left(g\sin\Theta_0\right)\theta + Z_u u + \\ &\quad + Z_v v + ... + Z_{\delta_{ped}}\Delta\delta_{ped} + Z_{\delta_{col}}\Delta\delta_{col} \end{aligned} \tag{37}$$

where state and control vectors are the perturbations near the trim

$$\begin{bmatrix} u \\ v \\ w \\ p \\ q \\ r \\ \phi \\ \theta \end{bmatrix} = \begin{bmatrix} U \\ V \\ W \\ P \\ Q \\ R \\ \Phi \\ \Theta \end{bmatrix} - \begin{bmatrix} U_0 \\ 0 \\ W_0 \\ 0 \\ 0 \\ 0 \\ \Phi_0 \\ \Theta_0 \end{bmatrix} \tag{38}$$

$$\begin{bmatrix} \Delta\delta_{ped} \\ \Delta\delta_{lat} \\ \Delta\delta_{lon} \\ \Delta\delta_{col} \end{bmatrix} = \begin{bmatrix} \delta_{ped} \\ \delta_{lat} \\ \delta_{lon} \\ \delta_{col} \end{bmatrix} - \begin{bmatrix} \delta_{ped_0} \\ \delta_{lat_0} \\ \delta_{lon_0} \\ \delta_{col_0} \end{bmatrix} \tag{39}$$

The right side of equations (37) consists of fluctuations of specific aerodynamic, gravitational, and inertial forces. We can calculate the perturbation of specific aerodynamic forces by eliminating the components related to gravity and kinematic relations from linearized equations.

$$\begin{aligned} \Delta\bar{X}_a &= X_u u + X_v v + ... + X_{\delta_{col}}\Delta\delta_{col} \\ \Delta\bar{Y}_a &= Y_u u + Y_v v + ... + Y_{\delta_{col}}\Delta\delta_{col} \\ \Delta\bar{Z}_a &= Z_u u + Z_v v + ... + Z_{\delta_{col}}\Delta\delta_{col} \end{aligned} \tag{40}$$

In Equation (40), the dimensional stability and control derivatives are just the partial derivatives of the specific aerodynamic forces to variations in the states and controls. In instance, $X_u \equiv (1/m)(\partial X_a/\partial u)$ and $X_{\delta_{col}} \equiv (1/m)(\partial X_a/\partial \delta_{col})$. Dimensional perturbations of the aerodynamic force vector are obtained by multiplying the equation (40) by a value of helicopter mass m for which a linear model has been identified.

$$\Delta\boldsymbol{F}_a = \begin{bmatrix} \Delta X_a \\ \Delta Y_a \\ \Delta Z_a \end{bmatrix} = \begin{bmatrix} m & & \\ & m & \\ & & m \end{bmatrix} \begin{bmatrix} \Delta\bar{X}_a \\ \Delta\bar{Y}_a \\ \Delta\bar{Z}_a \end{bmatrix} \tag{41}$$

Equation (41) is the perturbations around the aerodynamic trim force vector. Therefore, it should be summed with a trim value to get the total aerodynamic force vector.

$$\boldsymbol{F}_a = \Delta\boldsymbol{F}_a + \boldsymbol{F}_{a_0} \tag{42}$$

In the trim condition, the acceleration is zero, and therefore the equations (34) and (36) imply that

$$\boldsymbol{F}_{a_0} = \begin{bmatrix} m & & \\ & m & \\ & & m \end{bmatrix} \begin{bmatrix} g\sin\Theta_0 \\ -g\sin\Phi_0\cos\Theta_0 \\ -g\cos\Phi_0\cos\Theta_0 \end{bmatrix} \tag{43}$$

Finally, the specific aerodynamic force vector for the current helicopter mass m_c, which may be different from that for which the aerodynamic model was obtained, is calculated as

$$\bar{\boldsymbol{F}}_a = \begin{bmatrix} m_c & & \\ & m_c & \\ & & m_c \end{bmatrix}^{-1} \boldsymbol{F}_a \tag{44}$$

Moment Equations

The moment equation expressed in a body-fixed frame is

$$\frac{\partial\boldsymbol{H}}{\partial t} = -(\boldsymbol{\omega}\times\boldsymbol{H}) + \boldsymbol{M}_a \tag{45}$$

Since the coordinate system was chosen so that the rotorcraft is symmetric about $X-Z$ plane, we have

$$\boldsymbol{I} = \begin{bmatrix} I_x & 0 & -I_{xz} \\ 0 & I_y & 0 \\ -I_{zx} & 0 & I_z \end{bmatrix} \tag{46}$$

and $\begin{bmatrix}\dot{P} & \dot{Q} & \dot{R}\end{bmatrix}^T =$

$$= \boldsymbol{I}^{-1} \begin{bmatrix} (I_y - I_z)QR + I_{xz}PQ + L \\ (I_z - I_x)PR + I_{xz}(R^2 - P^2) + M \\ (I_x - I_y)PQ - I_{xz}QR + N \end{bmatrix} \tag{47}$$

The aerodynamic moment vector is calculated from the identified linear helicopter model. Similarly, for the force equations, we define the stability and control derivatives as $M_u \equiv (1/I_y)(\partial M/\partial u)$. The linearized equations are

$$\begin{aligned} \dot{p} &= L'_u u + L'_v v + L'_w w + ... + L'_{\delta_{col}}\delta_{col} \\ \dot{q} &= M_u u + M_v v + M_w w + ... + M_{\delta_{col}}\delta_{col} \\ \dot{r} &= N'_u u + N'_v v + N'_w w + ... + N'_{\delta_{col}}\delta_{col} \end{aligned} \tag{48}$$

where for the roll and yaw equations, the primed derivatives contain cross-coupled terms in form $L'_u \equiv (L_u + (I_{xz}/I_x)N_u)/(1 - I_{xz}^2/(I_z I_x))$. Since the whole moment in the trim is zero, it is sufficient to multiply the linearized equations (48) by the inertia tensor to obtain the total aerodynamic moment vector.

$$\boldsymbol{M}_a = \begin{bmatrix} L \\ M \\ N \end{bmatrix} = \boldsymbol{I} \begin{bmatrix} L'_u u + L'_v v + ... + L'_{\delta_{col}}\delta_{col} \\ M_u u + M_v v + ... + M_{\delta_{col}}\delta_{col} \\ N'_u u + N'_v v + ... + N'_{\delta_{col}}\delta_{col} \end{bmatrix} \tag{49}$$

The Euler rates in terms of the roll, pitch and yaw rates are expressed as

$$\begin{bmatrix} \dot{\Phi} \\ \dot{\Theta} \\ \dot{\Psi} \end{bmatrix} = \frac{1}{\cos\Theta}\Gamma \begin{bmatrix} P \\ Q \\ R \end{bmatrix} \tag{50}$$

where

$$\Gamma = \begin{bmatrix} \cos\Theta & \sin\Phi\sin\Theta & \cos\Phi\sin\Theta \\ 0 & \cos\Phi\cos\Theta & -\sin\Phi\cos\Theta \\ 0 & \sin\Phi & \cos\Phi \end{bmatrix} \tag{51}$$

DCM

The total transformation expression from inertial to body frame is

$$\boldsymbol{S}_I^B = \begin{bmatrix} c\Psi c\Theta, & s\Psi c\Theta, & -s\Theta \\ c\Psi s\Theta s\Phi - s\Psi c\Phi, & s\Psi s\Theta s\Phi + c\Psi c\Phi, & c\Theta s\Phi \\ c\Psi s\Theta c\Phi + s\Psi s\Phi, & s\Psi s\Theta c\Phi - c\Psi s\Phi, & c\Theta c\Phi \end{bmatrix} \tag{52}$$

where c and s denote the cosine and sine functions.

Helicopter Linear Model

The helicopter dynamics model used in the UKF has been identified for the following conditions: airspeed 30 knots, helicopter takeoff weight 35 kg, and AMSL 840 feet (256 m). The state space matrices in (8) have the following structure

$$
\boldsymbol{A} = \left[\begin{array}{c|c|c}
\multicolumn{1}{c|}{\boldsymbol{A}_{6\times6}} & \begin{array}{c}\boldsymbol{A}_{3\times2}\\ \\ \boldsymbol{0}_{3\times2}\end{array} & \boldsymbol{A}_{6\times2}\\
\hline
\begin{array}{cccc}\boldsymbol{0}_{3\times3} & \begin{array}{ccc}1 & 0 & \tan\Theta_0\\ 0 & 1 & 0\\ 0 & 0 & 1/\cos\Theta_0\end{array}\end{array} & \boldsymbol{0}_{3\times2} & \boldsymbol{0}_{3\times2}\\
\hline
\begin{array}{ccc}\boldsymbol{0}_{2\times3} & \begin{array}{cc}0 & 1\\ 1 & 0\end{array} & \boldsymbol{0}_{2\times1}\end{array} & \boldsymbol{0}_{2\times2} & \boldsymbol{A}_{2\times2}
\end{array}\right]
$$

where $\boldsymbol{0}$ is the null matrix and

$$
\boldsymbol{A}_{6\times6} = \begin{bmatrix}
X_u & X_v & X_w & X_p & X_q-W_0 & X_r\\
Y_u & Y_v & Y_w & Y_p+W_0 & Y_q & Y_r-U_0\\
Z_u & Z_y & Z_w & Z_p & Z_q+U_0 & Z_r\\
L'_u & L'_v & L'_w & 0 & 0 & L'_r\\
M_u & M_v & M_w & 0 & 0 & M_r\\
N'_u & N'_v & N'_w & N'_p & N'_q & N'_r
\end{bmatrix}
$$

$$
\boldsymbol{A}_{3\times2} = \begin{bmatrix}
0 & -g\cos\Theta_0\\
g\cos\Theta_0 & 0\\
0 & -g\sin\Theta_0
\end{bmatrix}
$$

$$
\boldsymbol{A}_{6\times2} = \begin{bmatrix}
X_{\beta_{1c}} & 0\\
0 & Y_{\beta_{1s}}\\
0 & 0\\
0 & L_{\beta_{1s}}\\
M_{\beta_{1c}} & 0\\
0 & 0
\end{bmatrix}
$$

$$
\boldsymbol{A}_{2\times2} = \begin{bmatrix}
-1/\tau_s & M_{f_{\beta_{1s}}}/\tau_s\\
L_{f_{\beta_{1c}}}/\tau_s & -1/\tau_s
\end{bmatrix}
$$

$$
\boldsymbol{B} = \begin{bmatrix}
X_{ped} & 0 & 0 & X_{col}\\
Y_{ped} & 0 & 0 & Y_{col}\\
Z_{ped} & Z_{lat} & Z_{lon} & Z_{col}\\
L'_{ped} & 0 & 0 & L'_{col}\\
M_{ped} & 0 & 0 & M_{col}\\
N'_{ped} & 0 & 0 & N'_{col}\\
0 & 0 & 0 & 0\\
0 & 0 & 0 & 0\\
0 & M_{f_{\delta_{lat}}}/\tau_s & M_{f_{\delta_{lon}}}/\tau_s & 0\\
0 & L_{f_{\delta_{lat}}}/\tau_s & L_{f_{\delta_{lon}}}/\tau_s & 0\\
0 & 0 & 0 & 0
\end{bmatrix}
$$

The numerical values of stability and control derivatives, as well as the trim values in (38)-(39), were provided by Steadicopter Ltd., and are not part of the studies in Technion IIT.

8. REFERENCES

[1] Dobrolenskiy, Y. P., "Flight Dynamics in Moving Air," NASA TT F-600, 1971, pp. 186–214.

[2] Osborne, J. and Rysdyk, R., "Waypoint Guidance for Small UAVs in Wind," Infotech@Aerospace, Arlington, VA, September 26-29, 2005.

[3] Anon, "Unmanned Aircraft System Roadmap (UAS). Circular 328," ICAO, 2011.

[4] Mayer, S., Hattenberger, G., Brisset, P., Jonassen, M., and Reuder, J., "A 'No-Flow-Sensor' Wind Estimation Algorithm for Unmanned Aerial Systems," *International Journal of Micro Air Vehicles*, Vol. 4 (1), 2012, pp. 15-30. DOI: `10.1260/1756-8293.4.1.15`.

[5] Khadeeja, T. N. and Singh, J., "Wind Profile Estimation during Flight Path Reconstruction," *Defence Science Journal*, Vol. 70 (3), 2020, pp. 231-239. DOI: `10.14429/dsj.70.13596`.

[6] Hajiyev, C., Cilden-Guler, D., and Hacizade, U., "Two-Stage Kalman Filter for Estimation of Wind Speed and UAV States by using GPS, IMU and Air Data System," *WSEAS Transactions on Electronics*, Vol. 10, 2019, pp. 60-65.

[7] Cho, A., Kim, J., Lee, S., and Kee, C., "Wind Estimation and Airspeed Calibration using a UAV with a Single-Antenna GPS Receiver and Pitot Tube," *IEEE Transactions on Aerospace and Electronic Systems*, Vol. 47 (1), Jan. 2011, pp. 109-117. DOI: `10.1109/TAES.2011.5705663`.

[8] Palomaki, R. T., Rose, N. T., Bossche, M. van den, Sherman, T. J., and Wekker, S. F. J. D., "Wind Estimation in the Lower Atmosphere Using Multirotor Aircraft," *Journal of Atmospheric and Oceanic Technology*, Vol. 34 (5), May 2017, pp. 1183-1191. DOI: `10.1175/JTECH-D-16-0177.1`.

[9] Schiano, F., Alonso-Mora, J., Rudinz, K., Beardsleyx, P., Siegwart, R., and Siciliano, B., "Towards Estimation and Correction of Wind Effects on a Quadrotor UAV," International Micro

Air Vehicle Conference and Competition, Delft, Netherlands, August 12-14, 2014.

[10] Meier, K., Hann, R., Skaloud, J., and Garreau, A., “Wind Estimation with Multirotor UAVs,” *Atmosphere*, Vol. 13 (4), 2022, ISSN: 2073-4433. DOI: 10.3390/atmos13040551. [Online]. Available: https://www.mdpi.com/2073-4433/13/4/551.

[11] Kumar, A. and Ben-Tzvi, P., “Estimation of Wind Conditions Utilizing RC Helicopter Dynamics,” *IEEE/ASME Transactions on Mechatronics*, Vol. 24 (5), 2019, pp. 2293-2303. DOI: 10.1109/TMECH.2019.2937844.

[12] Bergamasco, M., Ragazzi, A., and Lovera, M., “Rotorcraft System Identification: a Time/Frequency Domain Approach,” The 19th World Congress, Cape Town, South Africa, August 24-29, 2014.

[13] Etkin, B., *Dynamics of Atmospheric Flight*. Wiley, New York, NY, 1972, pp. 529–563.

[14] Cornman, L. B., “Airborne in situ measurements of turbulenc,” in *Aviation Turbulence: Processes, Detection, Prediction*, edited by R. Sharman and T. Lane, Chap. 5, Springer, Switzerland, 2016, pp. 97–120.

[15] Gool, P. van, “Rotorcraft responses to atmospheric turbulence,” Ph.D. dissertation, Delft University, 1997.

[16] George, V. V., Gaonkar, G. H., Prasad, J. V. R., and Schrage, D. P., “Adequacy of Modeling Turbulence and Related Effects on Helicopter Response,” *AIAA Journal*, Vol. 30 (6), Jun. 1992, pp. 1468-1479. DOI: 10.2514/3.11088.

[17] Mazurov, G. I. and Nesteruk, V. N., *The Weather Conditions and Helicopter Flights*, (in Russian). Hydrometeoizdat, Saint Petersburg, 1992, pp. 77–107.

[18] Volodko, A. M., *Fundamentals of Helicopter Aerodynamics and Dynamics*, (in Russian). Transport, Moscow, 1988, pp. 279–284.

[19] Schafer, S. A., “Flight test measurement of ship airwake disturbances using small-scale rotorcraft,” M.S. thesis, The Pennsylvania State University, 2015.

[20] Horn, J. F., Bridges, D. O., and Lee, D., “Flight Control Design for Alleviation of Pilot Workload during Helicopter Shipboard Operations,” American Helicopter Society 62nd Annual Forum, Phoenix, AZ, May 9-11, 2006.

[21] Sharman, R., “Nature of aviation turbulence,” in *Aviation Turbulence: Processes, Detection, Prediction*, edited by R. Sharman and T. Lane, Chap. 1, Springer, Switzerland, 2016, pp. 3–30.

[22] Cooke, M. V., *Flight Dynamics Principles*, 3rd, Elsevier, Oxford, 2013, pp. 443–446.

[23] Tischler, M. B. and Remple, R. K., *Aircraft and Rotorcraft System Identification: Engineering Methods with Flight Test Examples*, 2nd, AIAA, Reston, VA, 2012, pp. 20–21.

[24] Mansur, M. H., Tischler, M. B., Bacon, J. W., Cheung, K. K., Berrios, M. G., and Rothman, K. E., “Full Flight Envelope Inner-loop Control Law Development for the Unmanned K-MAX,” American Helicopter Society 67th Annual Forum, Virginia Beach, May, 2011.

[25] Tobias, E. L. and Tischler, M. B., “A Model Stitching Architecture for Continuous Full Flight-Envelope Simulation of Fixed-Wing Aircraft and Rotorcraft from Discrete-Point Linear Models,” AMRDEC, Spetial Report RDMR-AF-16-01, 2016.

[26] Gaonkar, G. H. and Hohenemser, K. H., “An Advanced Stochastic Model for Threshold Crossing Studies of Rotor Blade Vibrations,” *AIAA Journal*, Vol. 10 (8), 1972, pp. 1100-1101. DOI: 10.2514/3.50309.

[27] Leishman, J. G., *Principles of Helicopter Aerodynamics*, 2nd, Cambridge University Press, New York, NY, 2006, pp. 178–183.

[28] Simon, D., *Optimal State Estimation*. Wiley, Hoboken, NJ, 2006, pp. 433–457.

[29] Julier, S. J., “The Scaled Unscented Transformation,” Proceedings of the 2002 American Control Conference (IEEE Cat. No.CH37301), Anchorage, AK, May 08-10, 2002.

[30] Julier, S. J. and Uhlmann, J. K., “Unscented Filtering and Nonlinear Estimation,” *Proceedings of the IEEE*, Vol. 92 (3), Mar. 2004, pp. 401-422. DOI: 10.1109/JPROC.2003.823141.